Confined variational calculation of low-energy Ps-Li$^+$ scattering

D.-X. Zhao [1,2] M.-S. Wu,[3,*] J.-Y. Zhang [1,†] Z.-C. Yan,[4,1] and K. Varga[5]

[1]*State Key Laboratory of Magnetic Resonance and Atomic and Molecular Physics, Innovation Academy for Precision Measurement Science and Technology, Chinese Academy of Sciences, Wuhan 430071, China*

[2]*School of Physical Sciences, University of Chinese Academy of Sciences, Beijing 100049, China*

[3]*Center for Theoretical Physics, Hainan University, Haikou 570228, China*

[4]*Department of Physics, University of New Brunswick, Fredericton, New Brunswick, Canada E3B 5A3*

[5]*Department of Physics and Astronomy, Vanderbilt University, Nashville, Tennessee 37235, USA*

(Received 28 November 2023; accepted 29 February 2024; published 1 April 2024)

A theoretical investigation is conducted on the *s*- and *p*-wave elastic scatterings of positronium by a lithium ion Li$^+$ with the scattering energy below 1.41 eV, corresponding to the threshold of the e^+-Li channel. The confined variational method is applied to serve as the theoretical framework for this study. To accurately account for correlations between involved particles, explicitly correlated Gaussians are employed as basis functions, which are optimized through a hybrid approach combining stochastic variational and energy-gradient-based methods. Additionally, a straightforward yet effective algorithm is developed for the automatic adjustment of confining potentials. The *s*-wave zero-energy pickoff annihilation parameter $^1Z_{\mathrm{eff},0}$ is accurately determined to be 0.126 ± 0.002, which yields an enhancement factor of 1.88 compared with the value 0.067 obtained using the fixed-core stochastic variational method [Phys. Rev. A **65**, 034709 (2002)]. Finally, a broad *p*-wave resonance structure is predicted at the incident energy of approximately 0.27 eV, with the annihilation parameter $^1Z_{\mathrm{eff},1}$ at the resonance center estimated to be around 0.034.

DOI: 10.1103/PhysRevA.109.042801

I. INTRODUCTION

Positronium (Ps), consisting of an electron and its antiparticle positron, forms a hydrogenlike neutral system. Because Ps is exclusively leptonic, it serves as an ideal platform for investigating bound-state quantum electrodynamics [1,2], fundamental symmetries such as charge-parity and charge-parity-time symmetries [3–5], and new physics beyond the standard model [6]. Compared to typical neutral atoms, Ps exhibits stronger interactions with various forms of matter due to its small mass. As a result, it proves to be a promising tool for studying material characteristics in the field of material science. For example, Ps has been employed to investigate defects in diverse materials [7], providing valuable insights into their structural and dynamic properties. Moreover, experiments have been conducted to explore surface properties of alkali-metal crystals such as LiF by measuring Ps specular reflection [8,9]. In these investigations, a fundamental understanding of the interaction between Ps and other forms of matter, particularly the scattering process, is crucial.

The theoretical investigation of Ps scattering poses great challenges, primarily stemming from the intricate internal structures of both the positronium and the target. Describing these composite systems *ab initio* is computationally demanding. The coincidence of the center of mass and charge of Ps results in Coulomb interactions that are significantly weaker than the intricate short-range exchange correlations between Ps and the target, necessitating meticulous consideration. Adding to the complexity, the exchange matrix involving multicenter integrals proves to be challenging to evaluate, as highlighted by previous work [10]. Furthermore, Ps scattering exhibits distinct behaviors across various energy ranges, demanding tailored treatment approaches. In the intermediate-energy range, the scattering is predominantly governed by the exchange interaction between the electron and target. This is attributed to the inherently weak binding and diffuse nature of Ps, leading to striking similarities in total cross sections between Ps and e^- scattering across diverse atoms and molecules [11]. The elucidation of these similarities was provided by Fabrikant and Gribakin using the impulse approximation [12]. However, at lower energies, both short-range exchange and correlation interactions and long-range interactions come into play. Consequently, theories designed for low-energy Ps scattering must possess the capability to accurately describe these interactions.

Several theoretical approaches have been employed in the calculation of Ps scattering, including the many-body theory [13,14], the close-coupling method [15], the static-exchange method [16], and the Kohn variational method [17,18]. Another approach to tackle Ps scattering problem at low energies is the confined variational method (CVM). It was originally pioneered by Mitroy *et al.* [19] to address low-energy elastic scattering of electrons (or positrons). Subsequently, Zhang *et al.* extended the CVM to investigate low-energy elastic collisions between two internally structured systems [20,21], while Wu and co-workers advanced the approach to

*mswu@hainanu.edu.cn

†jzhang@apm.ac.cn

efficiently eliminate unphysical confining effects and extended its application to cases involving nonzero partial-wave scattering and higher collision energies [22,23]. The foundation of the CVM lies in the concept that two Hamiltonian operators, when subjected to the same confining potential and producing eigenenergies corresponding to the same scattering energy, yield identical phase shifts upon removing the confining potential. Consequently, the phase shifts of a many-body scattering system can be extracted by constructing an equivalent one-dimensional model potential and numerically solving its scattering equation.

Despite extensive theoretical and experimental investigations into Ps scattering by helium [13,22,24–27], studies focusing on Ps-Li^+ are relatively scarce, particularly in the low-energy range. Existing research on Ps-Li^+ primarily centers around intermediate- and higher-energy regimes. For example, Mukherjee and Ghosh [28] utilized the first-order Born approximation to explore elastic and excitation processes in Ps-Li^+ collisions. The Ps fragmentation process was investigated by Roy and Sinha within the framework of the postcollisional Coulomb distorted eikonal approximation [29]. Furthermore, Sur *et al.* [30], employing the coupled static close-coupling approximation, calculated elastic and electron capture cross sections in Ps-Li^+ collisions. Theoretical investigations into low-energy Ps-Li^+ scattering bear significance in the context of experimental detection of weakly bound state. The pioneering exploration of near-threshold scattering for Ps-Li^+ was conducted by Ivanov *et al.* [31] using the fixed-core stochastic variational method (FCSVM) and the stabilization concept [32,33] to derive the phase shift. However, the FCSVM has been found to underestimate the pickoff annihilation parameter $^1Z_{\rm eff}$ by an enhancement factor of approximately 2. This discrepancy arises from the neglect of correlations between the positron and electrons originating from the Li^+ core, which significantly affect the annihilation process [34]. Additionally, the FCSVM study is confined to the s wave, indicating the need to extend the analysis. To address these limitations and establish a benchmark for both theory and experiment, a rigorous all-electron CVM calculation for low-energy elastic Ps-Li^+ scattering becomes crucial.

In this paper, we present a detailed study of low-energy Ps-Li^+ scattering without the fixed-core approximation in the frame of the CVM. To enhance the efficiency of the CVM, we employ an energy optimization strategy combining both the stochastic variational and energy-gradient-based methods. Additionally, an algorithm is developed for the automatic adjustment of confining potentials. With these approaches, accurate phase shifts, cross sections, scattering length, and pickoff annihilation parameters are determined and compared with the results obtained using the fixed-core approximation. Notably, a broad p-wave resonance structure near threshold is observed and the impact of it on the cross sections and pickoff annihilation is analyzed.

II. THEORY

The Hamiltonian incorporating an artificial confining potential for Ps-Li^+ scattering, within the framework of the infinite-nuclear-mass approximation, can be expressed as

$$H = -\frac{1}{2}\sum_{i=1}^{4}\nabla_i^2 + \sum_{i=1}^{4}\frac{Qq_i}{r_i} + \sum_{j>i=1}^{4}\frac{q_iq_j}{r_{ij}} + \sum_{i=1}^{3}V_{\rm CP}(\rho_i), \tag{1}$$

where $Q = 3$ is the lithium nuclear charge; q_i is the ith lepton charge; $\boldsymbol{r}_1$, $\boldsymbol{r}_2$, and $\boldsymbol{r}_3$ are the position vectors of the three electrons relative to the fixed nucleus; $\boldsymbol{r}_4$ is the position vector of the positron; $r_{ij} = |\mathbf{r}_i - \mathbf{r}_j|$; and $\boldsymbol{\rho}_i = (\boldsymbol{r}_i + \boldsymbol{r}_4)/2$ is the position vector of the center of mass between the positron and the ith electron. Furthermore, $V_{\rm CP}(\rho_i)$ is an artificial confining potential, defined as

$$V_{\rm CP}(\rho_i) = \begin{cases} 0, & \rho_i < \rho_0 \\ G(\rho_i - \rho_0)^2, & \rho_i \geqslant \rho_0, \end{cases} \tag{2}$$

where G is an adjustable positive confining parameter and ρ_0 denotes the confining radius. It is crucial for ρ_0 to be sufficiently large to guarantee that the short-range interactions between Ps and Li^+ can be safely disregarded beyond this radius. To derive its matrix elements for variational calculation, it is more convenient to rewrite $V_{\rm CP}$ in terms of the relative coordinates $\boldsymbol{r}_i$ through the 4×1 matrix $\boldsymbol{r} \equiv (\boldsymbol{r}_1, \boldsymbol{r}_2, \boldsymbol{r}_3, \boldsymbol{r}_4)^T$,

$$V_{\rm CP}(\rho_i) = \begin{cases} 0, & \rho_i < \rho_0 \\ G\int \delta\big(\boldsymbol{W}_i^T\boldsymbol{r} - \boldsymbol{\xi}\big)(|\boldsymbol{\xi}| - \rho_0)^2 d\boldsymbol{\xi}, & \rho_i \geqslant \rho_0, \end{cases} \tag{3}$$

where $\boldsymbol{W}_i$ is a 4×1 matrix that transforms $\boldsymbol{r}$ into vector $\boldsymbol{\rho}_i$, for instance, $\boldsymbol{W}_1 = (\frac{1}{2}, 0, 0, \frac{1}{2})^T$ for $\boldsymbol{\rho}_1$.

For the s- and p-wave scatterings, the many-body confined wave function Ψ_c can be expanded in terms of the explicitly correlated Gaussian (ECG) basis functions [35,36]

$$\begin{aligned} \phi_k^{l=0}(\boldsymbol{r}, \boldsymbol{s}) &= \hat{P}\exp[-\boldsymbol{r}^T(\boldsymbol{A}_k \otimes \boldsymbol{I}_3)\boldsymbol{r}]\chi(\boldsymbol{s}), \\ \phi_k^{l=1}(\boldsymbol{r}, \boldsymbol{s}) &= \hat{P}z_{m_k}\exp[-\boldsymbol{r}^T(\boldsymbol{A}_k \otimes \boldsymbol{I}_3)\boldsymbol{r}]\chi(\boldsymbol{s}), \end{aligned} \tag{4}$$

where $\hat{P}$ is the permutation operator, $\boldsymbol{I}_3$ is a 3×3 identity matrix, and z_{m_k} refers to the z coordinate of the m_kth lepton. Also, $\chi(\boldsymbol{s})$ is the spin function with $\boldsymbol{s} \equiv (\boldsymbol{s}_1, \boldsymbol{s}_2, \boldsymbol{s}_3, \boldsymbol{s}_4)^T$ a column matrix containing all lepton spins. Further, $\boldsymbol{A}_k$ is the nonlinear parameter matrix expressed in the Cholesky decomposition form $\boldsymbol{A}_k = \boldsymbol{L}_k\boldsymbol{L}_k^T$, where $\boldsymbol{L}_k$ is a lower triangular matrix.

In the collision of Ps as a projectile, the confinement acts on the center of mass of the positron and each electron, which causes unphysical effects, i.e., the confinement onto the pseudopositronium formed by the positron and electron of Li^+. These unphysical effects become more pronounced at higher energy or angular momentum, where the orbital radius of Ps increases and the confinement becomes more intense. To effectively eliminate these unphysical effects, the following judgment indices [22] can be applied to determine the appropriate course of action:

$$\mathcal{S}_i^{kl} = \frac{\langle\phi_k|\Theta(r_{i4} - R_a)(r_{i4} - R_a)^2|\phi_l\rangle}{\langle\phi_k|\Theta(\rho_i - \rho_0)(\rho_i - \rho_0)^2|\phi_l\rangle}. \tag{5}$$

Here Θ is the Heaviside function, $r_{i4} = |\boldsymbol{r}_i - \boldsymbol{r}_4|$ is the distance between the positron and the ith electron, and R_a is an adjustable radius greater than the characteristic size $2a_0$ of Ps, where a_0 is the Bohr radius. If an electron in pseudopositronium under confinement originates from Li^+, the value of r_{i4} will be much greater than $2a_0$. This implies that when R_a is

properly set, $\mathcal{S}_i^{kl}$ will be significantly large. Consequently, the undesired confining effect can be eliminated by disregarding $\langle\phi_k|V_{\rm CP}(\rho_i)|\phi_l\rangle$ when $\mathcal{S}_i^{kl}$ exceeds a specific threshold. In this study, R_a is set to be equal to ρ_0 and the threshold for $\mathcal{S}_i^{kl}$ is set to 1.0.

The most-time-consuming procedures in the CVM involve optimizing basis functions and adjusting the confining parameter to match the total energy E_t of the scattering system. This energy is calculated as the sum of the incident energy E_s, the ground-state energy of Ps ($E_{\rm Ps}$), and the ground-state energy of Li^+ ($E_{\rm Li^+}$). The detailed introduction of energy optimization and confinement adjustment can be found in Sec. III. Given the confinement parameter G, one can adjust the one-dimensional model potential by solving the Schrödinger equation under the same confinement [19]

$$\left(-\frac{1}{2\mu}\frac{d^2}{d\rho^2}+\frac{l(l+1)}{2\mu\rho^2}+V_m(\rho)+V_{\rm CP}(\rho)\right)\psi_c^l(\rho) = E_s\psi_c^l(\rho), \tag{6}$$

where $\mu = 2$ is the reduced mass of the Ps-Li^+ system and $\psi_c^l(\rho)$ is the one-dimensional bound-state wave function of the l partial wave. The model potential $V_m(\rho)$ is chosen as

$$V_m(\rho) = \lambda\exp(-a\rho) - \frac{\alpha_d}{2\rho^4}[1-\exp(-\rho^6/b^6)], \tag{7}$$

where in the first term λ is adjustable and $a = 0.5$. The second term of Eq. (7) represents the long-range polarization potential between Ps and Li^+, in which $\alpha_d = 36a_0^3$ is the dipole polarizability of the ground-state Ps and b is the cutoff parameter. The primary reason for including the long-range potential in Eq. (7) is to ensure a correct description of the long-range tail and the effect of it in the interaction region can be recovered by adjusting λ [23]. Therefore, the results are not sensitive to the choice of b and we set $b = 5.0$. After determining the model potential, the confining potential can be removed, allowing the wave function to propagate under the influence of the model potential V_m with the logarithmic-derivative algorithm [37] to the boundary, and then match with the asymptotic solutions to extract the CVM phase shifts.

III. ENERGY OPTIMIZATION AND ADJUSTMENT OF CONFINING POTENTIAL

The accuracy of the CVM heavily relies on the choice of variational strategies. This is particularly true for complex systems like Ps-Li^+, where electron-electron and electron-positron correlations play a significant role. To address this challenge, a hybrid approach combining the stochastic variational method [31,38,39] and the energy-gradient-based method [35,36,40–43] is employed. This allows for the generation and optimization of basis functions by leveraging the strengths of these different methods.

To obtain the analytical expression for the energy gradient, we can start by considering the differential of the secular equation $(\boldsymbol{H}-E\boldsymbol{S})\boldsymbol{c} = 0$,

$$d[(\boldsymbol{H}-E\boldsymbol{S})\boldsymbol{c}] = d(\boldsymbol{H})\boldsymbol{c} - (dE)\boldsymbol{S}\boldsymbol{c} - E(d\boldsymbol{S})\boldsymbol{c} + (\boldsymbol{H}-E\boldsymbol{S})d\boldsymbol{c}, \tag{8}$$

where $\boldsymbol{H}$ and $\boldsymbol{S}$ are the $N\times N$ Hamiltonian and overlap matrices, respectively, and $\boldsymbol{c}$ is the N-dimensional vector of linear variational coefficients. Multiplying Eq. (8) by $\boldsymbol{c}^\dagger$ from the left gives rise to

$$dE = \boldsymbol{c}^\dagger(d\boldsymbol{H} - Ed\boldsymbol{S})\boldsymbol{c}. \tag{9}$$

For the real basis functions considered here, the energy derivative with respect to the nonlinear parameters a_k in the kth basis function can be written as

$$\frac{\partial E}{\partial a_k} = 2\sum_{\ell=1}^{N} c_k c_\ell\left(\frac{\partial H_{k\ell}}{\partial a_k} - E\frac{\partial S_{k\ell}}{\partial a_k}\right) - c_k^2\left(\frac{\partial H_{kk}}{\partial a_k} - E\frac{\partial S_{kk}}{\partial a_k}\right). \tag{10}$$

Only the derivatives with respect to the nonlinear parameters in matrices $\boldsymbol{L}_k$ and $\boldsymbol{L}_\ell$ are required. The final formulas for the matrix elements of the confining potential and their corresponding derivatives are provided in the Appendix. The formulas for matrix elements and corresponding derivatives of other related operators can be found in Refs. [35,36]. We employ the quasi-Newton method to minimize the energy and determine the grid steps along the search directions using the backtracking method [44]. To prevent being trapped in local minima, the SVM is applied after each round of gradient-based optimization.

During the energy optimization process, the CVM calculation necessitates accurately adjusting the confining parameter to obtain the total energy E_t of the scattering system [19,45]. However, manually adjusting it each time after optimizing the basis becomes arduous and cumbersome. To address this, an automated adjustment algorithm has been developed to fine-tune the confining parameter G. We first calculate the derivative of energy with respect to the variable G,

$$\frac{\partial E}{\partial G} = \sum_{k=1}^{N}\sum_{\ell=1}^{N} c_k c_\ell\frac{\partial (V_{\rm CP})_{k\ell}}{\partial G} = \left\langle\Psi_c(G)\left|\frac{\partial V_{\rm CP}}{\partial G}\right|\Psi_c(G)\right\rangle = \langle\Psi_c(G)|\Theta(\rho-\rho_0)(\rho-\rho_0)^2|\Psi_c(G)\rangle, \tag{11}$$

where $\Psi_c(G)$ stands for the wave function corresponding to the parameter G. The above relation is equivalent to the Hellmann-Feynman theorem [46]. As the derivative $\frac{\partial E}{\partial G} \geqslant 0$, it is evident that the energy E increases monotonically with an increase in G. Consequently, we initiate the optimization process with $G = 0$. Once the optimized energy E falls below a certain threshold value, we automatically search for a new value of G, denoted by G_1, such that $E(G_1) = E_t$. At this point, we continue optimizing the basis to further decrease the energy and adjust G_1 to G_2 using the reoptimized basis functions, ensuring that $E(G_2) = E_t$. This procedure is repeated for a specified number of iterations until the energy difference is within a predefined tolerance range. The monotonicity relationship between G and E guarantees that increasing G_i to G_{i+1} brings the confining parameter closer to the exact solution.

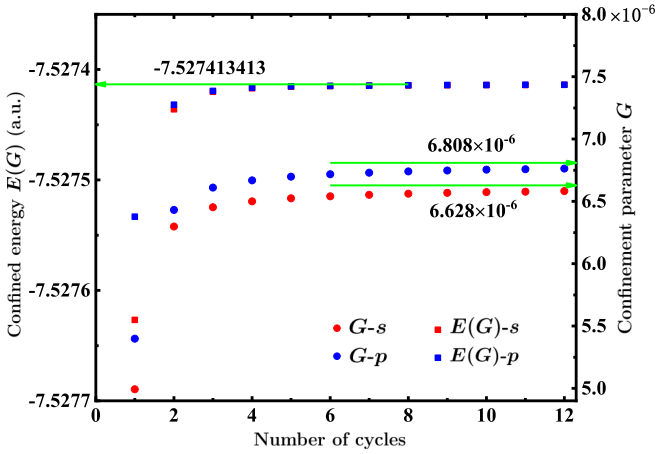

FIG. 1. Convergence of the confining parameter G and the total energy $E(G)$ for the s- and p-wave scatterings at the incident momentum $k = 0.1a_0^{-1}$ along with the optimization cycles based on the algorithm of Sec. IV.

IV. RESULTS AND DISCUSSION

A. Phase shifts and cross sections

In the present CVM calculation, we use the confining radius $\rho_0 = 20a_0$, the ground-state Ps energy $E_{\rm Ps} = -0.25$ a.u., and the ground-state Li^+ energy $E_{Li^+} = -7.279\,913\,413$ a.u. To validate the effectiveness of the automatic adjustment algorithm for the confining potential, we conduct a convergence analysis of the confining parameter G and the total energy $E(G)$ across multiple optimization cycles. During the test, the basis size remains fixed at 2400 and the energy is minimized solely using the gradient-based algorithm. Being initialized to zero, the confining parameter G is automatically adjusted after each cycle of optimization. Figure 1 illustrates the convergence behavior of G and $E(G)$ for both the s- and p-wave scatterings at $k = 0.1a_0^{-1}$ as the number of optimization cycles increases. For the p-wave scattering, the lowest energy level is optimized. However, in the case of s-wave scattering, the second lowest energy level is optimized instead. This is due to the presence of an s-wave bound state at the lowest energy level. The energies for the initial basis sets are $-7.529\,440\,207$ and $-7.529\,158\,557$ a.u. for the s wave and p wave, respectively. During the optimization process, the values of G and $E(G)$ steadily approach 6.628×10^{-6} and $-7.274\,134\,38$ a.u., respectively, for the s wave. For the p-wave scattering, the values converge to 6.808×10^{-6} and $-7.274\,134\,26$ a.u., respectively. This convergence can be observed in Fig. 1, where both energies gradually approach the desired energy of $E_t = -7.527\,413\,413$ a.u. Table I provides further evidence of convergence, as it demonstrates the convergence for the s- and p-wave scattering at $k = 0.1a_0^{-1}$ by increasing the size N of the ECG basis set. The parameters G of confining potentials, λ of the model potentials, and phase shifts $\delta^l_{0.1}$ all converge to the fourth significant digit for both s- and p-wave scattering. The results from Fig. 1 and Table I provide strong support for the effectiveness of the algorithms used in energy-gradient-based optimization, as well as the automatic adjustment of the confining potential.

TABLE I. Convergence of the s- and p-wave Ps-Li^+ scatterings at $k = 0.1a_0^{-1}$ as the number of ECG functions N increases. Here G is the adjustable parameter in the confining potential, $E(G)$ the total energy, λ the parameter in the model potential, and δ_l the l-wave phase shift. Note that $a^b = a \times 10^b$.

N	G	$E(G)$	λ	δ_l (rad)
		s-wave scattering		
2400	6.628^{-6}	−7.527413438	−0.03786	−1.1925
2800	6.634^{-6}	−7.527413425	−0.03794	−1.1918
3200	6.638^{-6}	−7.527413418	−0.03802	−1.1913
3600	6.639^{-6}	−7.527413414	−0.03802	−1.1913
		p-wave scattering		
2400	6.808^{-6}	−7.527413426	−0.05763	0.2107
2800	6.813^{-6}	−7.527413421	−0.05805	0.2112
3200	6.818^{-6}	−7.527413419	−0.05853	0.2118
3600	6.820^{-6}	−7.527413415	−0.05870	0.2120

Using the CVM, we calculate the s- and p-wave phase shifts $\delta_l(k)$ for incident energies below the threshold of the e^+-Li channel. Performing variational calculations directly for each incident momentum k is extremely time consuming. Therefore, we first optimize the bases for the specific momenta listed in Table II. The parameter λ in the model potential and the phase shift for each of these momenta are also shown in Table II. Additionally, we carry out calculations for the other momenta in their vicinity using these well-optimized bases as the initial bases. As shown in Fig. 2, the s-wave phase shifts obtained with the CVM exhibit great consistency with the results from both the FCSVM [47] and the hyperspherical close-coupling method (HSCC) [48]. These two methods employ the frozen-core approximation for Li^+, where the electron-core and positron-core interactions are approximated with model potentials. The differences among all three methods are within 5%, which demonstrates the effectiveness of

TABLE II. The s- and p-wave phase shifts for specific momenta below the threshold of the e^+Li channel, as well as the targeted energy levels and parameters λ in model potentials. Values in parentheses show estimated uncertainty due to the finite size of the ECG basis.

$k(a_0^{-1})$	Level	λ	CVM	FCSVM [47]	HSCC [48]
			s-wave phase shift		
0.05	2	−0.037632	−0.671(1)	−0.67	−0.65
0.10	2	−0.038022	−1.191(0)	−1.21	−1.18
0.20	2	−0.023030	−1.916(2)	−1.87	−1.86
0.30	3	−0.019277	−2.340(0)	−2.37	−2.34
0.40	4	−0.002262	−2.673(0)	−2.67	−2.70
			p-wave phase shift		
0.05	1	−0.027383	0.044(2)		
0.10	1	−0.058697	0.212(0)		
0.20	2	−0.081993	0.788(0)		
0.30	3	−0.100257	0.992(2)		
0.40	4	−0.112043	0.946(3)		

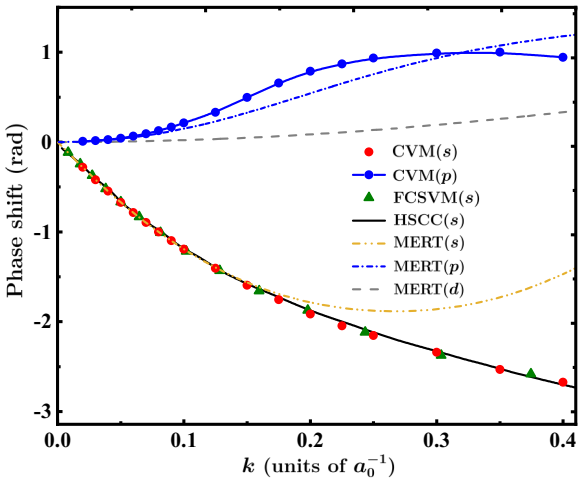

FIG. 2. Phase shifts for Ps-Li$^+$ scattering as a function of incident momentum k in units of a_0^{-1}. The following denotations are used: red (blue) circles, CVM s-wave (p-wave) phase shifts; green triangles, FCSVM s-wave phase shifts [47]; black solid line, HSCC s-wave phase shifts [48]; yellow dash–double-dotted line, s-wave phase shifts obtained by fitting the CVM phase shifts in the range of $k \leqslant 0.1a_0^{-1}$ to the MERT value in Eq. (18); and blue dash-dotted blue (gray dashed) line, p-wave (d-wave) phase shifts obtained with the MERT estimation of Eq. (12).

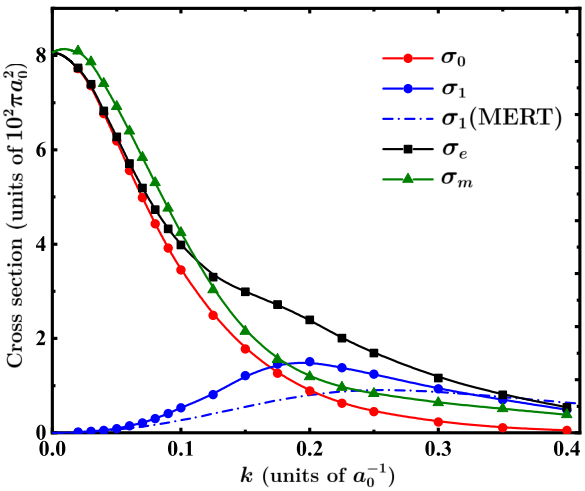

FIG. 3. Cross sections for Ps-Li$^+$ scattering as a function of incident momentum k in units of a_0^{-1}. The following denotations are used: red (blue) circles, CVM s-wave (p-wave) cross section; blue dash-dotted line, p-wave cross section obtained with the MERT estimation of Eq. (12); and black squares (green triangles), total elastic (momentum transfer) cross sections.

this frozen-core approximation for Ps-Li$^+$ elastic scattering. This is reasonable since the polarizability of Li$^+$ is $0.1925a_0^3$, which is negligible compared to the Ps polarizability of $36a_0^3$, and thus Li$^+$ is barely distorted during the elastic scattering at low energies. However, this is not the case for processes associated with pickoff annihilation, where the correlation among the positron and core electrons plays a significant role. Therefore, the enhancement factor due to the fixed-core approximation would eventually lead to an underestimation of the annihilation [34].

Compared to the s-wave phase shifts, higher partial wave phase shifts are significantly smaller near the zero-energy threshold. For example, at $k = 0.05a_0^{-1}$, the magnitude of the p-wave phase shift is approximately 15 times smaller than that of the s-wave phase shift, as shown in Table II. This can be attributed to the presence of the l-wave centrifugal barrier, which separates the asymptotic region, where the phase shift is determined by the asymptotic solution, from the interaction region. As a result, the phase shifts are suppressed as k approaches zero. When considering the presence of a polarization potential, the phase shifts of the lth ($l \geqslant 1$) partial wave can be estimated using the modified effective range theory (MERT) [49–51]:

$$\tan\delta_l = \frac{\mu\pi\alpha_d k^2}{(2l-1)(2l+1)(2l+3)}. \tag{12}$$

The MERT values of p-wave and d-wave phase shifts are depicted in Fig. 2. It can be observed that the MERT d-wave phase shifts remain small throughout the entire energy range considered and therefore the contribution from the $l \geqslant 2$ waves is not taken into account. The CVM p-wave results exhibit good agreement with the MERT values for $k < 0.1a_0^{-1}$. However, for $0.1a_0^{-1} \leqslant k \leqslant 0.3a_0^{-1}$, there is a relatively rapid increase in the phase shifts, leading to a deviation from the MERT values. This sudden rise in phase shifts gives rise to a resonance structure in the elastic cross section. In order to visualize the characteristic shape of this structure, we proceed to calculate the total elastic cross section

$$\sigma_e(k) = \sum_l \sigma_l(k) \approx \frac{4\pi}{k^2}\sum_{l=0}^{1}(2l+1)\sin^2\delta_l(k), \tag{13}$$

where $\sigma_l(k)$ is the l-wave cross section. Figure 3 shows that the s-wave cross section σ_0 increases rapidly towards the zero-energy threshold. This behavior is attributed to the presence of a weakly bound state in the s wave, which is represented by a pole of the S matrix located on the positive imaginary k axis. Furthermore, a wide peak is observed in σ_1 around $k = 0.2a_0^{-1}$, suggesting the possible existence of a resonance state. For incident momenta higher than that of the resonance peak, the p-wave cross section σ_1 dominates the total cross section σ_e and decelerates its decrease. Although the MERT phase shifts of Eq. (12) result in a broader shoulder feature in σ_1, they fail to reproduce the distinctive peak observed in the CVM data.

The Ps-Li$^+$ system exhibits interesting similarities to the e^+-Be and e^+-Zn systems [52–54]. One notable similarity is the significant increase in the s-wave cross section near the zero-energy threshold, which can be attributed to the presence of an s-wave bound state in each system [55]. In the low-energy scattering regime, the dominant influence is exerted by the long-range polarization potential, as the centrifugal barrier suppresses the impact of the short-range interaction. Furthermore, the dipole polarizabilities α_d of Be and Zn, specifically $37.8a_0^3$ [56] and $38.8a_0^3$ [57], respectively, are comparable to the $\alpha_d = 36a_0^3$ of Ps. Consequently, the p-wave cross sections of these systems also exhibit a similar resonance structure around the zero-energy threshold. It can be inferred that the low-energy scattering characteristics of

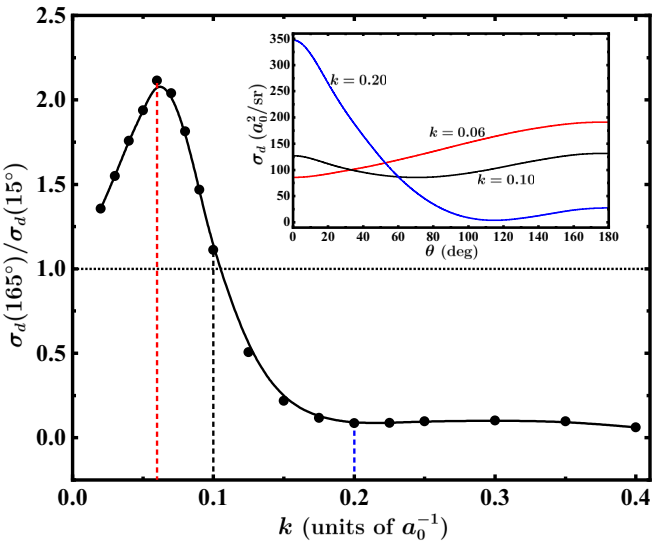

FIG. 4. Ratio of differential cross sections $\sigma_d(165^\circ)$ and $\sigma_d(15^\circ)$ as a function of k (units of a_0^{-1}). The inset provides a closer look at the relationship between the differential cross section and the angle θ.

Ps with other singly charged ions likely share these features, considering the dominant influence of Ps's polarizability and the ionization energies of the corresponding neutral atoms.

We also calculate the momentum transfer cross section

$$\sigma_m(k) = \frac{4\pi}{k^2}\sum_l (l+1)\sin^2[\delta_{l+1}(k)-\delta_l(k)]$$
$$\approx \frac{4\pi}{k^2}\{\sin^2[\delta_1(k)-\delta_0(k)] + 2\sin^2\delta_1(k)\}, \quad (14)$$

shown in Fig. 3. The line shape of σ_m is similar to that of σ_0 since the cross section is dominated by σ_0 near threshold. As the momentum approaches the zero-energy threshold, σ_m increases at a faster rate than σ_e. The rapid change of σ_m with respect to the incident energy, expressed as $d\sigma_m/dE$, below $k = 0.2a_0^{-1}$ (0.27 eV), strongly suggests the presence of an s-wave bound state of Ps-Li$^+$.

The presence of a positive scattering length (see in Sec. IV B) results in differential cross sections (DCSs) that are larger at backward angles compared to forward angles. This effect is particularly pronounced in systems with weakly bound states, as they have a larger scattering length. To quantify this, we calculate the DCS $\sigma_d(\theta)$ using the scattering amplitude $f(\theta)$, with $k \leqslant 0.4a_0^{-1}$,

$$\sigma_d(\theta) = |f(\theta)|^2, \quad (15)$$

where

$$f(\theta) = \frac{1}{2ik}\sum_l (2l+1)[\exp(2i\delta_l)-1]P_l(\cos\theta). \quad (16)$$

Phase shifts for $2 \leqslant l \leqslant 10$ can be estimated using the MERT as described in Eq. (12). In Fig. 4 we plot the DCS ratio $\sigma_d(165^\circ)/\sigma_d(15^\circ)$ as a function of k. It can be observed that the DCS ratio is greater than 1.0 when $k < 0.1a_0^{-1}$, reaching a maximum value of 2.1 at $k = 0.06a_0^{-1}$ (0.024 eV). However, the ratio drops below 0.1 for $k > 0.2a_0^{-1}$. Therefore, experimental measurement of DCS ratios can potentially provide evidence for the existence of a bound state in Ps-Li$^+$.

TABLE III. Comparison of s-wave scattering lengths a_s obtained using different methods, including the effective range theory [34], the model potential approach [47], the hyperspherical close-coupling method [48], the FCSVM [47], and the present CVM calculation fitted with ERT and MERT.

Method	k range	a_s (a.u.)
ERT[a]		10.1
model potential[b]		12.3
HSCC[c]	0.0–0.2	13.1
FCSVM (ERT)[b]	0.0–0.2	13.9
FCSVM (MERT)[b]	0.0–0.2	12.9
CVM (ERT)	0.0–0.1	14.2
CVM (MERT)	0.0–0.1	13.6

[a]Reference [34].
[b]Reference [47].
[c]Reference [48].

B. Scattering length

The scattering length plays a crucial role in determining the strength of the scattering process. In particular, it provides valuable insights into the interaction strength involved. When dealing with short-range interactions, one can determine the scattering length by employing the effective range theory (ERT) and performing a least-squares fitting of $\delta_0(k)$ at low incident momentum k [58],

$$k\cot\delta_0(k) = -\frac{1}{a_s} + \frac{R_0k^2}{2} + O(k^4), \quad (17)$$

where a_s is the s-wave scattering length and R_0 is the corresponding effective range. In addition, the MERT takes into account the effect of polarization [49,59–61],

$$k\cot\delta_0(k) = -\frac{1}{a_s} + \frac{\beta^2\pi k}{3a_s^2} + \frac{4\beta^2k^2}{3a_s}\ln\frac{\beta k}{4}$$
$$+ Bk^2 + Ck^3 + O(k^4), \quad (18)$$

where $\beta^2 = \mu\alpha_d(\mathrm{Ps}) = 72a_0^3$ [49], and B and C are two additional fitting parameters. Considering the uncertainties introduced by the fitting range, we conduct fitting for three different ranges $k \leqslant 0.08$, $k \leqslant 0.09$, and $k \leqslant 0.10$, which gives the average scattering length of 14.212 for the ERT and 13.613 for the MERT. Given the uncertainties inherent in the fitting procedure, we recommend a scattering length of 14.2 for the ERT and 13.6 for the MERT (see Table III). Mitroy and co-workers calculated a_s using ECGs together with the FCSVM [31,47]. In the present calculation, the fitting range of k is confined to within $0.1a_0^{-1}$, while for the FCSVM the fitting range is from 0.0 to $0.20a_0^{-1}$. The CVM ERT a_s is 4.4% and 10.1% larger than the CVM MERT and FCSVM MERT values, respectively. Moreover, the CVM MERT a_s is 34.7% larger than the value of $10.1a_0$ derived from the ERT formula $a_s = 1/\sqrt{2\mu|E_b|}$ using the binding energy E_b, and 10.6% larger than the value of $12.3a_0$ derived from the model potential estimation [47]. Considering these comparisons, the

scattering length obtained from the CVM MERT can be considered the most accurate one.

C. Pickoff annihilation

In Ps-Li^+ scattering, the primary decay mechanism is pickoff annihilation, which occurs when the positron annihilates with one of the target electrons, resulting in the emission of two photons. The pickoff annihilation cross section can be expressed as [34,62,63]

$$\sigma_a = 4\pi r_0^2 \left(\frac{c}{v}\right) {}^1Z_{\rm eff}, \tag{19}$$

where r_0 is the electron classical radius, c is the speed of light, and v is the velocity of incident Ps. Here ${}^1Z_{\rm eff}$ is a dimensionless parameter that represents the effective number of target electrons involved in the annihilation process. It can be expressed as the sum of annihilation parameters ${}^1Z_{{\rm eff},l}$ for different l partial waves:

$${}^1Z_{\rm eff}(k) = \sum_{l=0}^{\infty} {}^1Z_{{\rm eff},l}(k). \tag{20}$$

In terms of the confined l-wave many-body wave function Ψ_c^l, ${}^1Z_{{\rm eff},l}(k)$ can be written as

$${}^1Z_{{\rm eff},l}(k) = \frac{1}{|C_l|^2} \left\langle \Psi_c^l \middle| \sum_{i=1}^{3} \mathcal{P}_s(i,4)\delta(\boldsymbol{r}_i - \boldsymbol{r}_4) \middle| \Psi_c^l \right\rangle. \tag{21}$$

Here $\mathcal{P}_s(i,4)$ represents the spin projection operator that ensures only electron-positron pairs in a spin singlet state undergo annihilation. Also, the absolute value of C_l, the coefficient that normalizes Ψ_c^l to the asymptotic form, is defined as

$$|C_l|^2 = \frac{f(\rho_0)}{4\pi(2l+1)\rho_0^2[j_l(k\rho_0)\cos\delta_l - y_l(k\rho_0)\sin\delta_l]^2}, \tag{22}$$

where ρ_0 is the confinement radius, j_l and y_l are the spherical Bessel and Neumann functions, respectively, and $f(\rho)$ is the radial density distribution of Ps defined by

$$f(\rho) = \int d\Omega\, \rho^2 \langle \Psi_c^l | \delta(\boldsymbol{W}^T\boldsymbol{r} - \boldsymbol{\rho}) | \Psi_c^l \rangle, \tag{23}$$

with $\int d\Omega$ the integral over the solid angle of $\boldsymbol{\rho}$. It should be noted that the accuracy of such a calculation is limited due to less accurate local properties of variational wave functions compared to global properties [64]. To increase the accuracy of the calculated C_l, there are two alternative approaches that can be employed. The first approach involves using the wave function ψ_c^l of the one-dimensional potential scattering (6) instead of the many-body wave function Ψ_c^l [45]. In this approach, the model potential (7) is tuned to have the same scattering energy E_s and confining energy $\langle V_{\rm CP}\rangle$. By ensuring the same $\langle V_{\rm CP}\rangle$, the normalization conditions at the boundaries are also the same, allowing for the use of $\psi_c^l(\rho_0)$ to calculate C_l. This approach requires the model potential to be more flexible in order to easily perform the necessary adjustments, such as making the parameter a in Eq. (7) adjustable. The second approach involves using a stabilization idea to fit

$$f(\rho) = 4\pi(2l+1)C_l^2\rho^2[j_l(k\rho)\cos\delta_l - y_l(k\rho)\sin\delta_l]^2 \tag{24}$$

in the small interval $\rho \in [\rho_0 - d, \rho_0]$ with $d = 2.0a_0$ near the confining radius ρ_0. Then C_l is determined as a fitting parameter.

In addition, we also estimate the annihilation parameter ${}^1Z_{{\rm eff},0}(0)$ for the s-wave zero energy using the binding energy of the Ps-Li^+ bound state [65–68] and the core-annihilation rate based on the lowest-order ERT [34],

$${}^1Z_{{\rm eff},0}(0) \approx \frac{a_s^3\Gamma}{2r_0^2c} \approx \frac{1}{2r_0^2c}\frac{\Gamma}{|2\mu E_b|^{3/2}}, \tag{25}$$

where Γ is the core-annihilation rate and E_b is the binding energy. Expressing Γ in units of $\rm ns^{-1}$ leads to

$${}^1Z_{{\rm eff},0}(0) \approx 0.031\,12 \times \frac{\Gamma}{|2\mu E_b|^{3/2}}. \tag{26}$$

TABLE IV. Convergence of the total nonrelativistic energy E, the binding energy E_b with respect to the dissociation into the ground-state Ps and $Li^+(^1S)$, and the core-annihilation rate Γ, as the size of the basis set N increases.

N	E (a.u.)	E_b (a.u.)	Γ ($\rm ns^{-1}$)
2400	−7.53241006	0.00249666	0.0031352
3000	−7.53241054	0.00249714	0.0031784
3600	−7.53241057	0.00249717	0.0031839
4200	−7.53241064	0.00249724	0.0031854
1200[a]	−7.5323955	0.0024821	0.0030833
3000[b]	−7.53241048	0.00249708	
8568[c]	−7.27991341		

[a]ECG basis functions. From [65].
[b]ECG basis functions. From [69].
[c]The ground-state energy of Li^+ using the Hylleraas-CI method with 8568 configuration states. From [70].

Table IV presents the convergence of the nonrelativistic energy E of the Ps-Li^+ bound state, the binding energy E_b with respect to the dissociation, and the core-annihilation rate Γ. The binding energy is determined to be 0.002 497 24 hartree with 4200 well-optimized ECGs. The annihilation rate converges to 0.003 185 4 $\rm ns^{-1}$, which is 3.3% larger than the previous value of 0.003 083 3 $\rm ns^{-1}$ [65] obtained with 1200 ECGs. The value of ${}^1Z_{{\rm eff},0}(0)$ is determined to be 0.099, as shown in Table V, which is approximately 2.02 times the results of the FCSVM and 4.2% larger than the value obtained with the SVM. Additionally, ${}^1Z_{{\rm eff},0}(0)$ can be determined by extrapolating ${}^1Z_{{\rm eff},0}(k)$ to $k = 0$ utilizing the ERT expansion [71]

$${}^1Z_{{\rm eff},0}(k) = {}^1Z_{{\rm eff},0}^{(0)} + {}^1Z_{{\rm eff},0}^{(1)}k^2 + {}^1Z_{{\rm eff},0}^{(2)}k^4. \tag{27}$$

The extrapolation with ${}^1Z_{{\rm eff},0}(k)$ of the CVM in the ranges $0.02 \leqslant k \leqslant 0.10$, $0.03 \leqslant k \leqslant 0.10$, and $0.04 \leqslant k \leqslant 0.10$ yields values 0.127, 0.126, and 0.124, respectively, for ${}^1Z_{\rm eff}(0)$. We recommend using the average value ${}^1Z_{\rm eff}(0) = 0.126$ as the final result, and the uncertainty is within 0.002. Comparing with the FCSVM value of 0.067 [34], we can determine an enhancement factor of 1.88.

The energy dependence of ${}^1Z_{\rm eff}$ is crucial for understanding the thermalization process of positronium in gases [72–74]. Figure 5 illustrates the CVM ${}^1Z_{{\rm eff},0}(k)$ and ${}^1Z_{{\rm eff},1}(k)$ for $k \leqslant 0.4a_0^{-1}$. The CVM ${}^1Z_{{\rm eff},0}(k)$ is approximately twice the result

TABLE V. Comparison of the s-wave threshold pickoff annihilation parameters ${}^1Z_{\mathrm{eff},0}(0)$, calculated using different methods, including the lowest-order ERT estimation based on the binding energy and core-annihilation rate obtained by FCSVM [65], SVM [65], and the present bound-state calculation. Additionally, the extrapolation value using Eq. (27), based on the results of FCSVM [34] and the present CVM, is also provided. Here E_b represents the binding energy and Γ represents the core-annihilation rate.

Method	E_b (a.u.)	Γ (ns^{-1})	${}^1Z_{\mathrm{eff},0}(0)$
ERT (FCSVM)[a]	0.0024789	0.0015715	0.049
ERT (SVM)[a]	0.0024821	0.0030833	0.095
ERT[b]	0.0024972	0.0031854	0.099
extra (FCSVM)[c]			0.067
extra (CVM)			0.126

[a]Reference [65].
[b]Present work.
[c]Reference [34].

of the FCSVM, indicating that the FCSVM underestimates ${}^1Z_{\mathrm{eff}}(k)$ by an enhancement factor of about 2. On the other hand, ${}^1Z_{\mathrm{eff},0}(k)$ can be estimated in terms of ${}^1Z_{\mathrm{eff},0}(0)$ and the scattering length a_s using the formula [34]

$$ {}^1Z_{\mathrm{eff},0}(k) = \frac{{}^1Z_{\mathrm{eff},0}(0)}{1 + a_s^2 k^2}. \tag{28}$$

The energy dependence of ${}^1Z_{\mathrm{eff}}(k)$ at low energies is qualitatively described by Eq. (28), as shown in Fig. 5. However, this equation underestimates the values of ${}^1Z_{\mathrm{eff},0}(k)$. Moreover, ${}^1Z_{\mathrm{eff},1}(k)$ exhibits a peak at $k \approx 0.2a_0^{-1}$, similar to the p-wave cross section, as expected. However, determining the peak value of ${}^1Z_{\mathrm{eff},1}(k)$ is challenging due to the convergence difficulties near the peak. We determine the peak value to be 0.034 using 5000 ECGs. Although the p-wave contribution to annihilation surpasses that of the s wave for $k \geqslant 0.2a_0^{-1}$, the total annihilation parameter ${}^1Z_{\mathrm{eff},1}(k)$ only shows a subtle bump.

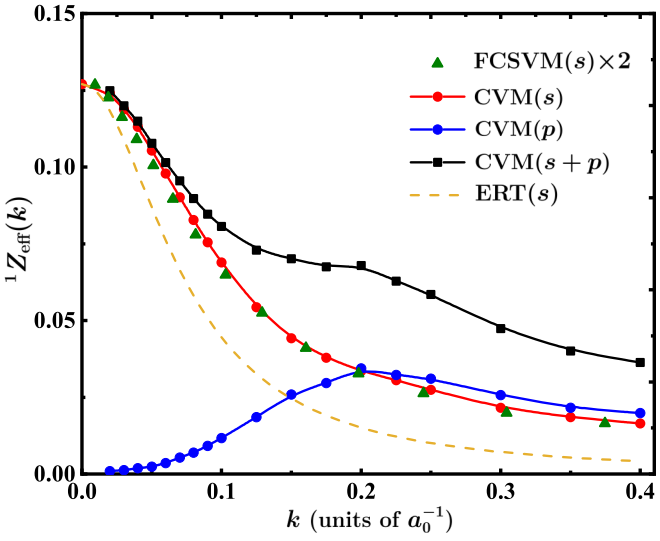

FIG. 5. Pickoff annihilation parameter ${}^1Z_{\mathrm{eff}}$ for the Ps-Li$^+$ scattering as a function of incident momentum k in units of a_0^{-1}. The red and blue solid circles are for the s- and p-wave scattering, respectively, using the CVM, and the black square is the total annihilation parameter. The green triangles represent the FCSVM results multiplied by 2 [34]. The yellow dashed line shows the ERT estimation of the s-wave annihilation parameter using Eq. (28).

V. SUMMARY

This study focused on the scattering of Ps by the ground-state Li$^+$ using the CVM. The variational calculation was performed by optimizing the basis through a hybrid approach combining stochastic variational and energy-gradient-based methods. Additionally, an algorithm was developed to automatically adjust the confining potentials. Both of the strategies greatly enhance the efficiency of scattering calculation in the frame of the CVM. Accurate phase shifts and cross sections were obtained and the scattering length was determined to be $13.6a_0$ by fitting the phase shifts to the MERT. Moreover, a broad p-wave resonance structure at $k \approx 0.2a_0^{-1}$ (0.27 eV) was predicted, displaying structures similar to those in e^+-Be and e^+-Zn scattering. It is anticipated that similar resonance structures will be observed in the scattering of e^+ with some other atoms and Ps with other ions. Finally, the energy dependence of pickoff annihilation was also investigated. The s-wave zero-energy pickoff annihilation parameter ${}^1Z_{\mathrm{eff},0}$ was accurately determined to be 0.126 ± 0.002, which is crucial for other frozen-core methods to determine the enhancement factor.

It is noteworthy that the weakly bound state of Ps-Li$^+$ has been extensively investigated in numerous theoretical studies [65–67], yet there is a noticeable absence of experimental detection. We have found that the momentum transfer cross section σ_m exhibits a significant change rate below 0.27 eV due to the presence of the s-wave bound state. Therefore, the measurement of $d\sigma_m/dE$ using either angular correlation of the annihilation radiation [25,75,76] or Doppler broadening spectroscopy [24,72,73] methods could provide evidence of the binding between Ps and Li$^+$. Furthermore, the differential cross section was found to be larger in the backward direction than in the forward direction near the threshold. This implies that the ratio of differential cross sections below 0.068 eV could also serve as evidence for the existence of the weakly bound state of Ps-Li$^+$.

ACKNOWLEDGMENTS

J.-Y.Z. is deeply indebted to S. Yi for valuable discussion and generous hospitality during his visit at the Institute of Theoretical Physics, Chinese Academy of Sciences. We thank G. F. Gribakin for helpful comments and advice. This work was supported by the National Natural Science Foundation of China under Grants No. 12174399, No. 12274106, and No. 11934014. M.-S.W. was supported by Hainan Provincial Natural Science Foundation of China under Grant No. 122MS005. Z.-C.Y. was supported by the Natural Sciences and Engineering Research Council of Canada (NSERC).

APPENDIX: MATRIX ELEMENTS AND GRADIENT FOR THE CONFINING POTENTIAL

By utilizing the matrix element expressions of the Dirac δ function as shown in Refs. [35,36], we can express the matrix elements of the confining potential in Eq. (3) between the kth and ℓth basis functions for the s and p waves (assuming the magnetic quantum number $m = 0$) as

$$(V_{\rm CP})^{l=0}_{k\ell} = GS_{k\ell}\alpha_1\Big[-\frac{\beta}{\sqrt{\pi}}\exp(-\beta^2) + \Big(\frac{3}{2}+\beta^2\Big) \times \mathrm{erfc}(\beta)\Big] \tag{A1}$$

and

$$(V_{\rm CP})^{l=1}_{k\ell} = GS_{k\ell}\alpha_1\Big[\frac{\beta}{\sqrt{\pi}}\Big(\frac{2}{3}\frac{\alpha_2}{\alpha_1\alpha_3}-1\Big)\exp(-\beta^2) + \Big(\frac{3}{2}+\beta^2+\frac{\alpha_2}{\alpha_1\alpha_3}\Big)\mathrm{erfc}(\beta)\Big], \tag{A2}$$

where $\mathrm{erfc}(\beta)$ is the complementary error function and $S_{k\ell}$ is the overlap matrix element. We also use the abbreviations

$$\alpha_1 = \mathrm{tr}\big[\boldsymbol{W}\boldsymbol{W}^T\tilde{\boldsymbol{A}}^{-1}_{k\ell}\big], \tag{A3}$$

$$\alpha_2 = \mathrm{tr}[\boldsymbol{W}\boldsymbol{W}^T\boldsymbol{K}_{k\ell}], \tag{A4}$$

$$\alpha_3 = \mathrm{tr}\big[\tilde{\boldsymbol{v}}^{\ell}(\boldsymbol{v}^k)^T\tilde{\boldsymbol{A}}^{-1}_{k\ell}\big], \tag{A5}$$

$$\beta = \frac{\rho_0}{\sqrt{\alpha_1}}, \tag{A6}$$

where

$$\tilde{\boldsymbol{A}}_{k\ell} = \boldsymbol{A}_k + \tilde{\boldsymbol{A}}_\ell, \quad \tilde{\boldsymbol{A}}_\ell = \boldsymbol{P}^T\boldsymbol{A}_\ell\boldsymbol{P}, \quad \tilde{\boldsymbol{v}}^{\ell} = \boldsymbol{P}^T\boldsymbol{v}^{\ell}, \tag{A7}$$

and

$$\boldsymbol{K}_{k\ell} = \tilde{\boldsymbol{A}}^{-1}_{k\ell}\tilde{\boldsymbol{v}}^{\ell}(\boldsymbol{v}^k)^T\tilde{\boldsymbol{A}}^{-1}_{k\ell}. \tag{A8}$$

In the above equations, $\boldsymbol{P}$ represents a permutation matrix for identical particles and $\boldsymbol{v}_k$ is a column vector where the m_kth component is equal to one while all other components are zero. By differentiating Eqs. (A1) and (A2) with respect to the nonlinear parameter matrices $\boldsymbol{L}_k$ and $\boldsymbol{L}_\ell$, respectively, we can obtain

$$\frac{\partial(V_{\rm CP})^{l=0}_{k\ell}}{\partial(\mathrm{vech}\boldsymbol{L})} = \frac{(V_{\rm CP})^{l=0}_{k\ell}}{S_{k\ell}}\frac{\partial S_{k\ell}}{\partial(\mathrm{vech}\boldsymbol{L})} + GS_{k\ell}\gamma_0\frac{\partial\alpha_1}{\partial\,\mathrm{vech}\boldsymbol{L}} \tag{A9}$$

and

$$\frac{\partial(V_{\rm CP})^{l=1}_{k\ell}}{\partial(\mathrm{vech}\boldsymbol{L})} = \frac{(V_{\rm CP})^{l=1}_{k\ell}}{S_{k\ell}}\frac{\partial S_{k\ell}}{\partial(\mathrm{vech}\boldsymbol{L})} + GS_{k\ell}\Big(\gamma_1\frac{\partial\alpha_1}{\partial\,\mathrm{vech}\boldsymbol{L}} + \gamma_2\frac{\partial\alpha_2}{\partial\,\mathrm{vech}\boldsymbol{L}} - \gamma_3\frac{\partial\alpha_3}{\partial\,\mathrm{vech}\boldsymbol{L}}\Big), \tag{A10}$$

where $\boldsymbol{L} = \boldsymbol{L}_k$ or $\boldsymbol{L}_\ell$ and

$$\begin{aligned}
\gamma_0 &= \frac{1}{\sqrt{\pi}}\beta\exp(-\beta^2) + \frac{3}{2}\mathrm{erfc}(\beta),\\
\gamma_1 &= \frac{1}{\sqrt{\pi}}\Big(\frac{2}{3}\frac{\alpha_2}{\alpha_1\alpha_3}(1+\beta^2)+1\Big)\beta\exp(-\beta^2) + \frac{3}{2}\mathrm{erfc}(\beta),\\
\gamma_2 &= \frac{1}{\alpha_3}\Big(\frac{2}{3\sqrt{\pi}}\beta\exp(-\beta^2) + \mathrm{erfc}(\beta)\Big),\\
\gamma_3 &= \frac{\alpha_2}{\alpha_3^2}\Big(\frac{2}{3\sqrt{\pi}}\beta\exp(-\beta^2) + \mathrm{erfc}(\beta)\Big).
\end{aligned} \tag{A11}$$

The operator vech transforms a matrix into a vector; for instance, if $\boldsymbol{L}$ is a 3×3 matrix, then

$$\mathrm{vech}\boldsymbol{L} = (L_{11}, L_{12}, L_{13}, L_{22}, L_{23}, L_{33})^T. \tag{A12}$$

The derivatives for α_1, α_2, and α_3 are

$$\begin{aligned}
\frac{\partial\alpha_1}{\partial(\mathrm{vech}\boldsymbol{L}_k)} &= -2\,\mathrm{vech}\Big[\Big(\tilde{\boldsymbol{A}}^{-1}_{k\ell}\boldsymbol{W}\boldsymbol{W}^T\tilde{\boldsymbol{A}}^{-1}_{k\ell}\Big)\boldsymbol{L}_k\Big],\\
\frac{\partial\alpha_1}{\partial(\mathrm{vech}\boldsymbol{L}_\ell)} &= -2\,\mathrm{vech}\Big[\boldsymbol{P}\Big(\tilde{\boldsymbol{A}}^{-1}_{k\ell}\boldsymbol{W}\boldsymbol{W}^T\tilde{\boldsymbol{A}}^{-1}_{k\ell}\Big)\boldsymbol{P}^T\boldsymbol{L}_\ell\Big],\\
\frac{\partial\alpha_2}{\partial(\mathrm{vech}\boldsymbol{L}_k)} &= -\mathrm{vech}\big[(\boldsymbol{M}_{k\ell}+\boldsymbol{M}^T_{k\ell})\boldsymbol{L}_k\big],\\
\frac{\partial\alpha_2}{\partial(\mathrm{vech}\boldsymbol{L}_\ell)} &= -\mathrm{vech}\big[\boldsymbol{P}(\boldsymbol{M}_{k\ell}+\boldsymbol{M}^T_{k\ell})\boldsymbol{P}^T\boldsymbol{L}_\ell\big],\\
\frac{\partial\alpha_3}{\partial(\mathrm{vech}\boldsymbol{L}_k)} &= -\mathrm{vech}\big[(\boldsymbol{K}_{k\ell}+\boldsymbol{K}^T_{k\ell})\boldsymbol{L}_k\big],\\
\frac{\partial\alpha_3}{\partial(\mathrm{vech}\boldsymbol{L}_\ell)} &= -\mathrm{vech}\big[\boldsymbol{P}(\boldsymbol{K}_{k\ell}+\boldsymbol{K}^T_{k\ell})\boldsymbol{P}^T\boldsymbol{L}_\ell\big],
\end{aligned} \tag{A13}$$

with

$$\boldsymbol{M}_{k\ell} = \boldsymbol{K}_{k\ell}\boldsymbol{W}\boldsymbol{W}^T\tilde{\boldsymbol{A}}^{-1}_{k\ell} + \tilde{\boldsymbol{A}}^{-1}_{k\ell}\boldsymbol{W}\boldsymbol{W}^T\boldsymbol{K}_{k\ell}. \tag{A14}$$

[1] G. Adkins, D. Cassidy, and J. Pérez-Ríos, Phys. Rep. **975**, 1 (2022).

[2] B. A. Kniehl, A. V. Kotikov, and O. L. Veretin, Phys. Rev. A **80**, 052501 (2009).

[3] W. Bernreuther, U. Löw, J. P. Ma, and O. Nachtmann, Z. Phys. C **41**, 143 (1988).

[4] T. Namba, K. Nishihara, T. Yamazaki, S. Asai, and T. Kobayashi, AIP Conf. Proc. **1037**, 56 (2008).

[5] T. Yamazaki, T. Namba, S. Asai, and T. Kobayashi, Phys. Rev. Lett. **104**, 083401 (2010).

[6] C. Frugiuele, J. Pérez-Ríos, and C. Peset, Phys. Rev. D **100**, 015010 (2019).

[7] T. Goworek, J. Nucl. Radiochem. Sci. **1**, 11 (2000).

[8] M. H. Weber, S. Tang, S. Berko, B. L. Brown, K. F. Canter, K. G. Lynn, A. P. Mills, L. O. Roellig, and A. J. Viescas, Phys. Rev. Lett. **61**, 2542 (1988).

[9] K. Michishio, L. Chiari, F. Tanaka, N. Oshima, and Y. Nagashima, JJAP Conf. Proc. **7**, 011304 (2018).
[10] H. S. W. Massey and C. B. O. Mohr, Proc. Phys. Soc. A **67**, 695 (1954).
[11] S. J. Brawley, S. Armitage, J. Beale, D. E. Leslie, A. I. Williams, and G. Laricchia, Science **330**, 789 (2010).
[12] I. I. Fabrikant and G. F. Gribakin, Phys. Rev. Lett. **112**, 243201 (2014).
[13] D. G. Green, A. R. Swann, and G. F. Gribakin, Phys. Rev. Lett. **120**, 183402 (2018).
[14] A. R. Swann, D. G. Green, and G. F. Gribakin, Phys. Rev. A **107**, 042802 (2023).
[15] J. E. Blackwood, M. T. McAlinden, and H. R. J. Walters, J. Phys. B: At. Mol. Opt. Phys. **35**, 2661 (2002).
[16] H. Ray and A. S. Ghosh, J. Phys. B: At. Mol. Opt. Phys. **29**, 5505 (1996).
[17] B. A. P. Page, J. Phys. B: At. Mol. Phys. **9**, 1111 (1976).
[18] P. V. Reeth and J. W. Humberston, J. Phys. B: At. Mol. Opt. Phys. **36**, 1923 (2003).
[19] J. Mitroy, J. Y. Zhang, and K. Varga, Phys. Rev. Lett. **101**, 123201 (2008).
[20] J.-Y. Zhang, Z.-C. Yan, and U. Schwingenschlögl, Europhys. Lett. **99**, 43001 (2012).
[21] J.-Y. Zhang, M.-S. Wu, Y. Qian, X. Gao, Y.-J. Yang, K. Varga, Z.-C. Yan, and U. Schwingenschlögl, Phys. Rev. A **100**, 032701 (2019).
[22] M.-S. Wu, J.-Y. Zhang, X. Gao, Y. Qian, H.-H. Xie, K. Varga, Z.-C. Yan, and U. Schwingenschlögl, Phys. Rev. A **101**, 042705 (2020).
[23] W. Du, M.-S. Wu, J.-Y. Zhang, Y. Qian, K. Varga, and Z.-C. Yan, Phys. Rev. A **105**, 052809 (2022).
[24] J. J. Engbrecht, M. J. Erickson, C. P. Johnson, A. J. Kolan, A. E. Legard, S. P. Lund, M. J. Nyflot, and J. D. Paulsen, Phys. Rev. A **77**, 012711 (2008).
[25] Y. Nagashima, T. Hyodo, K. Fujiwara, and A. Ichimura, J. Phys. B: At. Mol. Opt. Phys. **31**, 329 (1998).
[26] A. Basu, P. K. Sinha, and A. S. Ghosh, Phys. Rev. A **63**, 052503 (2001).
[27] P. K. Biswas and S. K. Adhikari, Phys. Rev. A **59**, 363 (1999).
[28] M. Mukherjee and A. S. Ghosh, Phys. Rev. A **46**, 2558 (1992).
[29] S. Roy and C. Sinha, Phys. Rev. A **80**, 022713 (2009).
[30] S. Sur, S. K. Adhikari, and A. S. Ghosh, Phys. Rev. A **53**, 3340 (1996).
[31] I. A. Ivanov, J. Mitroy, and K. Varga, Phys. Rev. Lett. **87**, 063201 (2001).
[32] R. J. Drachman and S. K. Houston, Phys. Rev. A **12**, 885 (1975).
[33] A. U. Hazi and H. S. Taylor, Phys. Rev. A **1**, 1109 (1970).
[34] I. A. Ivanov and J. Mitroy, Phys. Rev. A **65**, 034709 (2002).
[35] S. Bubin and L. Adamowicz, J. Chem. Phys. **124**, 224317 (2006).
[36] S. Bubin and L. Adamowicz, J. Chem. Phys. **128**, 114107 (2008).
[37] B. Johnson, J. Comput. Phys. **13**, 445 (1973).
[38] I. A. Ivanov, J. Mitroy, and K. Varga, Phys. Rev. A **65**, 032703 (2002).
[39] Y. Suzuki and K. Varga, *Stochastic Variational Approach to Quantum-Mechanical Few-Body Problems* (Springer, Berlin, 1998).
[40] S. Bubin, M. Pavanello, W.-C. Tung, K. L. Sharkey, and L. Adamowicz, Chem. Rev. **113**, 36 (2013).
[41] D. B. Kinghorn and L. Adamowicz, J. Chem. Phys. **110**, 7166 (1999).
[42] P. M. Kozlowski and L. Adamowicz, J. Chem. Phys. **97**, 5063 (1992).
[43] W.-C. Tung, M. Pavanello, K. L. Sharkey, N. Kirnosov, and L. Adamowicz, J. Chem. Phys. **138**, 124101 (2013).
[44] J. Nocedal and S. J. Wright, *Numerical Optimization*, edited by T. V. Mikosch, S. I. Resnick, and S. M. Robinson (Springer, New York, 1999), p. 37.
[45] J. Y. Zhang, J. Mitroy, and K. Varga, Phys. Rev. A **78**, 042705 (2008).
[46] R. P. Feynman, Phys. Rev. **56**, 340 (1939).
[47] J. Mitroy and I. A. Ivanov, Phys. Rev. A **65**, 012509 (2001).
[48] A.-T. Le, M. W. J. Bromley, and C. D. Lin, Phys. Rev. A **71**, 032713 (2005).
[49] T. F. O'Malley, L. Spruch, and L. Rosenberg, J. Math. Phys. **2**, 491 (1961).
[50] T. F. O'Malley, L. Rosenberg, and L. Spruch, Phys. Rev. **125**, 1300 (1962).
[51] O. Hinckelmann and L. Spruch, Phys. Rev. A **3**, 642 (1971).
[52] M. W. J. Bromley, J. Mitroy, and G. Ryzhikh, J. Phys. B: At. Mol. Opt. Phys. **31**, 4449 (1998).
[53] M. V. Barp, W. Tenfen, and F. Arretche, Atoms **11**, 8 (2023).
[54] J. Mitroy, J. Y. Zhang, M. W. J. Bromley, and S. I. Young, Phys. Rev. A **78**, 012715 (2008).
[55] M. W. J. Bromley and J. Mitroy, Phys. Rev. A **65**, 062506 (2002).
[56] J. Komasa, Phys. Rev. A **65**, 012506 (2001).
[57] D. Goebel, U. Hohm, and G. Maroulis, Phys. Rev. A **54**, 1973 (1996).
[58] *Springer Handbook of Atomic, Molecular, and Optical Physics*, edited by G. W. F. Drake (Springer, New York, 1982), p. 669.
[59] T. F. O'Malley and R. W. Crompton, J. Phys. B: At. Mol. Phys. **13**, 3451 (1980).
[60] Z. L. Petrovic, T. F. O'Malley, and R. W. Crompton, J. Phys. B: At. Mol. Opt. Phys. **28**, 3309 (1995).
[61] T. F. O'Malley, Phys. Rev. **130**, 1020 (1963).
[62] G. F. Gribakin, J. A. Young, and C. M. Surko, Rev. Mod. Phys. **82**, 2557 (2010).
[63] P. Fraser, Adv. At. Mol. Phys. **4**, 63 (1968).
[64] R. Krivec, V. B. Mandelzweig, and K. Varga, Phys. Rev. A **61**, 062503 (2000).
[65] J. Mitroy, Phys. Rev. A **70**, 024502 (2004).
[66] G. G. Ryzhikh and J. Mitroy, Phys. Rev. Lett. **79**, 4124 (1997).
[67] K. Strasburger and H. Chojnacki, J. Chem. Phys. **108**, 3218 (1998).
[68] G. G. Ryzhikh, J. Mitroy, and K. Varga, J. Phys. B: At. Mol. Opt. Phys. **31**, 3965 (1998).
[69] S. Bubin and O. V. Prezhdo, Phys. Rev. Lett. **111**, 193401 (2013).
[70] J. S. Sims, B. Padhy, and M. B. Ruiz, Int. J. Quantum Chem. **122**, e26823 (2022).
[71] J. Mitroy, Phys. Rev. A **66**, 022716 (2002).

[72] M. Skalsey, J. J. Engbrecht, R. K. Bithell, R. S. Vallery, and D. W. Gidley, Phys. Rev. Lett. **80**, 3727 (1998).

[73] M. Skalsey, J. J. Engbrecht, C. M. Nakamura, R. S. Vallery, and D. W. Gidley, Phys. Rev. A **67**, 022504 (2003).

[74] R. S. Vallery, A. E. Leanhardt, M. Skalsey, and D. W. Gidley, J. Phys. B: At. Mol. Opt. Phys. **33**, 1047 (2000).

[75] P. G. Coleman, S. Rayner, F. M. Jacobsen, M. Charlton, and R. N. West, J. Phys. B: At. Mol. Opt. Phys. **27**, 981 (1994).

[76] F. Saito, Y. Nagashima, and T. Hyodo, J. Phys. B: At. Mol. Opt. Phys. **36**, 4191 (2003).